Biosensors and Bioelectronics 131 (2019) 274–279

Contents lists available at ScienceDirect

Biosensors and Bioelectronics

journal homepage: www.elsevier.com/locate/bios

Novel electrochemical nanoswitch biosensor based on self-assembled pH-sensitive continuous circular DNA

Xian Chen[a,*], Le Yao[a], Yu-Chao Wang[a], Qin Chen[b], Hai Deng[c], Zhen-Yu Lin[a], Huang-Hao Yang[a,*]

[a] College of Chemistry, Fuzhou University, Fuzhou 350116, PR China
[b] Fujian Cancer Hospital & Fujian Medical University Cancer Hospital, Fuzhou 350014, PR China
[c] Department of Chemistry, School of Natural and Computing Sciences, University of Aberdeen, Aberdeen AB24 3UE, United Kingdom

ARTICLE INFO

Keywords:
Nanoswitch biosensor
PH-sensitive
Continuous circular DNA
Biosensor
Electrochemical biosensor
MiRNA detection

ABSTRACT

Nucleic acid nanoswitches have a status that cannot be ignored in the field of biosensing due to the excellent biocompatibility and flexibility of design. In our current research, we have constructed a new electrochemical platform based on self-assembled pH-sensitive continuous circular DNA nanoswitch for miRNA-21 detection. We elaborately designed an inside ring probe (IRP) which could form a circle when complemented with an outside ring probe (ORP). Under the weakly acidic condition, IRPs and ORPs are self-assembled into continuous annular DNA, meanwhile, the nanoswitch is activated. However, if it is not a weakly acidic environment with a pH equal to 6, these circles are separated and the nanoswitch cannot be triggered. Therefore, the biosensor doesn't work. Only when the pH is 6, can the nanoswitch be activated. Consequently, a large number of RuHex will accumulate on the continuous annular DNA, which leads to highly sensitive detection of miRNA-21, with concentration ranged from 10^{-15} to 10^{-8} M and limit of detection down to 0.84 fM. More importantly, this nanoswitch-based biosensor can directly detect the target microRNA in human serum without pretreatment. Therefore, the proposed novel electrochemical DNA nanoswitch will have broad application prospects in biomarker detection and clinical diagnosis.

1. Introduction

Nucleic acid nanoswitches are nucleic acid motifs that change between two (or more) conformations (usually "off" and "on") in response to a particular chemical or environmental input, depending on non-canonical DNA interaction (Desrosiers and Vallée-Bélisle, 2017; Iacovelli et al., 2017). Nucleic acid nanoswitches, based on DNA motifs such as aptamers, G-quadruplex and triplex-forming oligonucleotides (TFOs), are widely applied to biosensing (Lin et al., 2015; Xu et al., 2018; Zhao et al., 2013) and nanomedicine (Huang et al., 2016; Raftery et al., 2016; Smith et al., 2013). Among these DNA motifs, the TFOs display strong pH dependence. The structure of TFOs can reversibly fold/unfold by switching pH from acid to neutral. The formation of triplex DNA is based on the simple rule of Hoogsteen and Watson-Crick base pairings, which contains base triplets C-G•C+ and T-A•T (Idili et al., 2014; Liao and Willner, 2017). The protonation of the N3 of cytosine in the third strand requires an acid environment, while T-A•T structure needs a neutral condition (Wang et al., 2017). The unique properties of triple helix DNA make it ideal for the construction of pH-regulated nanoswitches. It has been demonstrated that slightly acidic pH is the optimum condition, in order to form a stable triplet DNA segment with an equal content of CGC vs. TAT (Xiong et al., 2017).

MicroRNA (miRNA) is a kind of small endogenous non-coding RNA consisting of approximately 22–25 nucleotides. MicroRNA can negatively regulate gene expression via translation inhibition, mRNA degradation and protein synthesis repression (Bartel, 2014; Lim et al., 2016; Liu et al., 2017; Zhou et al., 2016). So, the aberrant levels of miRNAs will influence various biological processes such as allergic diseases (Lu and Rothenberg, 2017), hematopoietic differentiation (Yin et al., 2012), cardiovascular diseases (Xu et al., 2012) and cancer (Sheu et al., 2010). The relationship between miRNA and tumor has been extensively studied. It has been reported that some miRNAs remarkably up-regulated in cervical cancer (Zaman et al., 2016), colon cancer (Hansen et al., 2014), non-small cell lung cancer (Wang et al., 2011), hidradenitis suppurativa (Hessam et al., 2017) and breast cancer (Qian et al., 2016). Therefore, miRNAs are increasingly becoming potential tumor markers for the diagnosis and prognostic of clinical diseases. It is increasingly urgent to find a rapid, sensitive and reliable method for detecting miRNAs.

Substantial research efforts have been performed about the highly

* Corresponding authors.
E-mail addresses: xchen_fzu@126.com (X. Chen), hhyang@fzu.edu.cn (H.-H. Yang).

https://doi.org/10.1016/j.bios.2019.02.004
Received 27 November 2018; Received in revised form 9 February 2019; Accepted 11 February 2019
Available online 20 February 2019
0956-5663/

sensitive detection of miRNA expression, including microarray-based techniques (Lee and Jung, 2011; Li et al., 2014; Tian et al., 2015), fluorescence (Le and Seo, 2018; Wei et al., 2017), Northern blotting (Jin et al., 2016; Válóczi et al., 2004; Várallyay et al., 2008) and quantitative reverse transcription polymerase chain reaction (qRT-PCR) (Hu et al., 2017; Jung et al., 2016; Kulcheski et al., 2010). Despite their novelty and high sensitivity, these methods have certain practical drawbacks, such as poor reproducibility, time-consuming, high cost and requirements for professional experimental skills. Recently, electrochemical detection methods have attracted widespread attention and been widely used in the detection of various biomarkers, due to their intrinsic low detection limit, high specificity and convenience. For instance, electrochemical methods have been used to detect adenosine triphosphate (Liu et al., 2014), microRNA (Chen et al., 2012; Yu et al., 2018), DNA (Chen et al., 2011; Fang et al., 2018; Xu et al., 2013) and tumor exosomes (Zhang et al., 2018).

Inspired by the above research, herein, we report a novel method for ultrasensitive electrochemical detection miRNA based on self-assembled pH-sensitive continuous circular DNA nanoswitch. In this study, we designed two probes for self-assembly, outside ring probe (ORP) and inside ring probe (IRP). Under the suitable pH condition, IRPs and ORPs can self-assemble into many DNA rings connected by TFOs. Therefore, a stable continuous annular DNA structure was formed and the nanoswitch was activated. We used electroactive Hexaammineruthenium (III) chloride ($[Ru(NH_3)_6]^{3+}$, RuHex) as the signal reporter. A large number of RuHex can electrostatically adsorb on the negatively charged continuous annular DNA. When targets are present, RuHex on the nanoswitch will lead to a significant electrochemical signal, named switch on. On the other hand, if the pH condition is not suitable, the nanoswitch will not be activated, which means the switch is off. Obviously, if there is no target in the system, the switch is also off. This strategy has several merits. Firstly, this is a "signal-on" strategy which could minimize false positive. Secondly, by changing the corresponding sequence in the capture probe, this strategy can be used to detect multiple target DNA or miRNA. What's more, it can achieve ultra-sensitive detection, which is attributed to the numerous RuHex electrostatic binding to the long continuous annular DNA. Last but not least, this TFOs nanoswitch is reversibly switchable in different pH environments, which makes it particularly suitable for monitoring of pH changes in cellular extracts or in vivo cells (Modi et al., 2009, 2013).

2. Experimental section

2.1. Materials and reagents

Tris (2-carboxyethyl) phosphine hydrochloride (TCEP, 98%), ethylene diamine tetraacetic acid (EDTA), hexaammineruthenium (III) chloride ([Ru (NH3)6]3 + , RuHex), 6-mercapto-1-hexanol (MCH), tris (hydroxymethyl) aminomethane were obtained from Sigma-Aldrich. All of the other chemicals are of analytical reagent grade and can be used without farther purification. HPLC-purified oligonucleotides were synthesized and purified by Sangon Biotechnology Co. Ltd. (Shanghai, China). All the oligonucleotide sequences used in this work are listed in Table S1.

2.2. Buffer solutions used in this work

A capture probe (CP) immobilization buffer (I -buffer, 10 mM Tris-HCl containing 10 mM TCEP, 1 mM EDTA and 500 mM NaCl) was used to dilute the CP. DNA hybridization buffer (H-buffer, 10 mM Tris-HCl containing 100 mM NaCl, 2.5 mM $MgCl_2$) was employed to dilute other oligonucleotides. A 10 mM Tris-HCl buffer containing 50 μM RuHex was used as the differential pulse voltammetry (DPV) test buffer (D-buffer). A 100 mM phosphate buffer solution (PBS) including 0.1 M KCl, 5 mM K_4 [Fe (CN) $_6$] and 5 mM K_3 [Fe (CN) $_6$] was used as the electrochemical impedance spectroscopy (EIS) test buffer (E-buffer). A 10 mM Tris-buffer (T-buffer) was used to rinse electrode before next-step modification. The pH of all the buffers mentioned above used in this experiment was 6 unless otherwise stated. Cyclic voltammetry (CV) test buffer (C-buffer) was prepared by 0.5 M H_2SO_4 and the blocking buffer by 2 mM MCH. Ultrapure water (18.2 MΩ•cm resistivity) obtained from a Millipore water system was used throughout the experiment.

2.3. Instrumentation

All electrochemical measurements were performed on a CHI660C electrochemical workstation (Chenhua Instruments Co., Ltd., Shanghai, China) at room temperature. A conventional three-electrode configuration was employed throughout the experiment, which comprised a gold working electrode (2 mm in diameter), a platinum wire auxiliary electrode and an Ag/AgCl reference electrode. CV tests, which were employed to characterize the electrode surface, were carried out in C-buffer with a potential range from − 0.35–1.6 V at a scan rate of 0.1 V/s. DPV experiments were performed by scanning the potential window from − 0.6–0.2 V with 0.05 V amplitude, 0.05 s pulse width and 0.5 s pulse period in D-buffer. EIS experiments were performed in E-buffer over a frequency range from 0.1 Hz to 10^5 Hz and 5 mV amplitude.

2.4. Preparation of the sensors

In the beginning, the Au electrode was immersed in a piranha solution (H_2SO_4: H_2O_2 = 3:1 v/v) for 20 min. After rinsed thoroughly with ultrapure water, the bare Au electrode was burnished carefully with 1, 0.3 and 0.05 μm aluminum powder to obtain a mirror plane. Then, the Au electrode was rinsed with ultrapure water and successive ultrasonic cleaned with ethanol and ultrapure water for 5 min respectively to remove the residual Al_2O_3 powder. Subsequently, the electrode was electrochemically cleaned with C-buffer of a potential range of − 0.35–1.6 V until a steady-state reproducible cyclic voltammogram was obtained. Ultimately, thoroughly rinse the well-prepared electrode with ultrapure water and dry it with nitrogen. Use it as soon as possible for probe immobilization.

2.5. Fabrication of the nanoswitch biosensor

Before experiments, CP (1 μM) in I-buffer was heated to 95 °C for 5 min, followed by slowly decreasing to room temperature for at least 2 h to form a hairpin structure. At the same time, ORP (5 μM) and IRP (5 μM) in H-buffer were heated to 95 °C for 5 min, followed by slowly cooling to room temperature as well. Then, the nanoswitch biosensor was fabricated as follow. At first, 10 μL of CP solution (1 μM) was dropped onto the surface of a cleaned Au electrode and incubated for 180 min in the dark. The CP oligomers can be immobilized on Au electrode surface (CP/Au) via gold-sulfur chemistry bond. Then, the electrode was thoroughly rinsed with T-buffer gently and dried under a stream of nitrogen gas. Afterward, to block the nonspecific binding sites of Au electrode and obtain well-organized DNA monomolecular layer, the CP/Au was incubated for 90 min with blocking buffer (10 μL). The resulting electrode, marked as MCH + CP/Au, was then rinsed with T-buffer and dried with nitrogen. Next, H-buffer (10 μL) containing target probes (TP) with different concentration was coated on the Au electrode (TP/MCH + CP/Au) for 60 min and subsequently rinsed with T-buffer. After that, 10 μL of linked probes (LP) was dropped on the above electrodes for 60 min self-assembly (LP/TP/MCH + CP/Au). The modified electrode was washed with T-buffer and dried under nitrogen. And then, 10 μL of H-buffer solution (pH 6) contained ORP and IRP was coated on Au electrode (ORP + IRP/LP/TP/MCH + CP/Au) for 60 min to form a complete nanoswitch biosensor. Prior to detection, the electrode, ORP + IRP/LP/TP/MCH + CP/Au, was placed in 10 mM Tris-HCl containing 50 μM RuHex (pH 6) for 2 min to reach the equilibrium

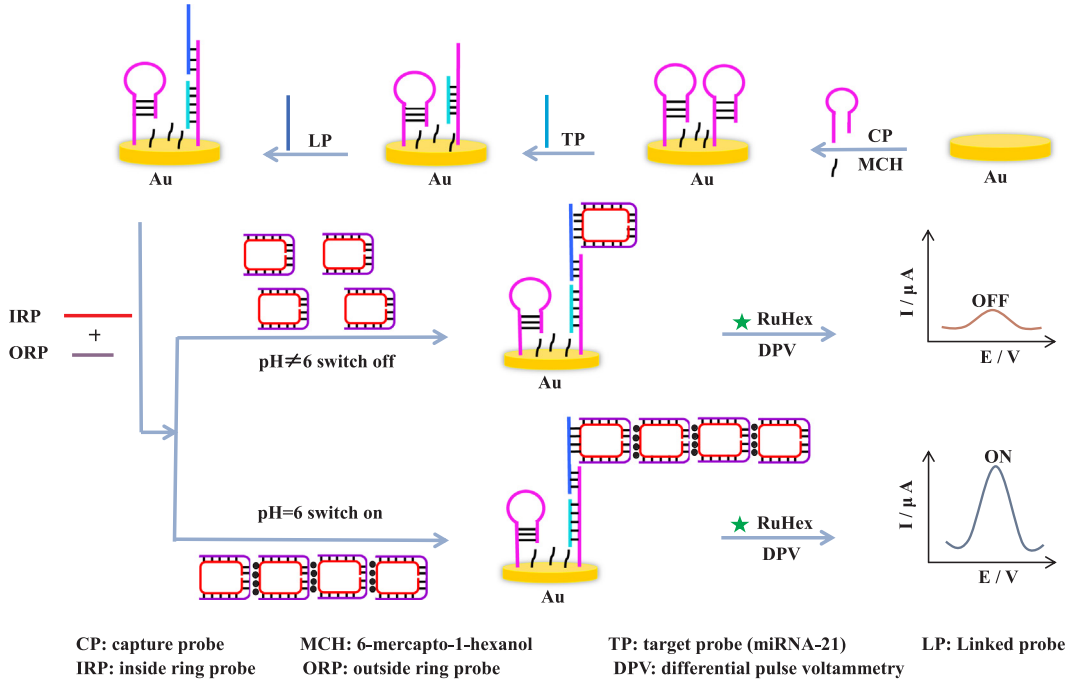

Scheme 1. Illustration of the novel electrochemical nanoswitch biosensor used for ultrasensitive detection of miRNA-21 based on self-assembled pH-sensitive continuous circular DNA.

adsorption of RuHex. Finally, the sensor was rinsed with T-buffer and moved to the electrochemical cell for measurement.

2.6. Real samples analysis

MiRNA-21 is up-regulated in the serum of breast cancer patients. We tried to detect the expression of miRNA-21 levels in serum of breast cancer patients. Serum samples from breast cancer patients and healthy volunteers were kindly supplied by Fujian Provincial Cancer Hospital (Fujian, China). The serum samples were diluted 2 times with ultrapure water and the detection method same as described above.

3. Results and discussion

3.1. The principle of the strategy

The mechanism of electrochemical nanoswitch biosensor based on self-assembled pH-sensitive continuous circular DNA is represented in Scheme 1. Firstly, in order to activate the pH-dependent nanoswitch, we take full advantage of the transition between duplex and triplex DNA in different pH environments. We tactfully designed two DNA sequences, ORP and IRP. Under alkaline buffer conditions, an ORP and an IRP can be self-assembled into a separate DNA ring. LP can be complementary to the single-stranded part of the DNA ring. One LP can be connected to only one ring. However, only under weakly acidic condition (pH 6), IRPs and ORPs can be self-assembled into continuous DNA rings connected by TFOs. The stably formed continuous annular DNA structure, which is used as a key component of nanoswitch and an excellent carrier for signal amplification, can be attached to CP via LP. CP, which is designed to be complementary to both TP and LP, can be immobilized on the Au electrode through thiol groups and form a hairpin structure after thermally annealed. In order to improve the quality and stability of CP on the electrode, we use MCH to block the nonspecific binding sites. In the absence of target miRNA-21, the predominant form of CP is hairpin structure. The binding force of LP and CP is insufficient to open the stem-loop structure of CP. However, in the presence of target miRNA-21, the hairpin structure of CP is unfolded, and the newly exposed sticky end of CP will hybridize with LP stably. LP plays the role of connecting the amplification probe (ORP + IRP) with CP. In this way, the complete nanoswitch biosensor is established. RuHex was selected as the electrochemical reporter. The more continuous annular DNA structures are self-assembled on the electrode, the more RuHex are bound. As such, the stronger signal is generated. In addition, since the formation of the DNA nanoswitch is independent of the base sequence of the target, if we change the complementary base sequence on the capture probe according to another target probe, the nanoswitch can also be used to detect other nucleic acid targets, which will have broad application prospects.

3.2. Characterization of the nanoswitch biosensor

As an effective measure for evaluating the interface characteristics of modified electrodes, electrochemical impedance spectroscopy (EIS) is usually employed to study the stepwise assembly process of the gold electrode. In a representative EIS, the cross section of the high frequency semicircle represents the charge transfer limiting process, and the diameter of the semicircle varies with the change of the resistance of the interfacial charge transfer (Rct) (Xu et al., 2017). As described in Fig. 1, the electron transfer resistance (Ret) of Au electrode modified with CP and MCH (curve b) was significantly increased compared with the undecorated Au electrode (curve a), which clearly indicated that CP fixed on the electrode surface already. Subsequently, when TP was hybridized with CP, an increased Ret (curve c) could be seen on account of the electrostatic repulsion between $[Fe(CN)_6]^{3-/4-}$ anions and negatively charged phosphate backbone of DNA. As expected, the Ret kept increasing with the modification of LP (curve d), proving the successful link between CP and LP. Notably, when IRP and ORP self-assembled to be continuous circular DNA on the gold electrode surface and connected with LP, a large number of negative charges were accumulated on the surface of the electrode and a significant steric hindrance was produced, which resulted in a significant increase in the diameter of the semicircle (curve e). Obviously, if IRP and ORP were not self-assembled to be continuous circular DNA, no large electrochemical impedance could be observed. These outcomes confirmed that the fabrication of electrochemical nanoswitch biosensor for miRNA assay was successful.

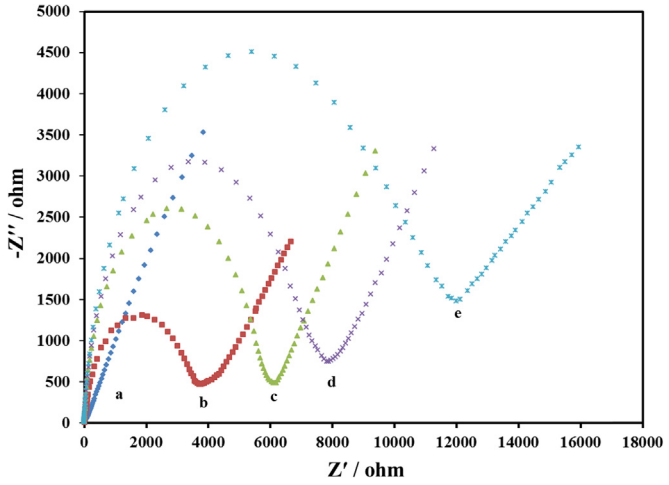

Fig. 1. EIS (Nyquist plots) of the gold electrodes modified with various oligonucleotides in the E-buffer: (a) bare Au electrode, (b) MCH + CP/Au, (c) TP/MCH + CP/Au, (d) LP/TP/MCH + CP/Au, (e) ORP + IRP/LP/ TP/MCH + CP/Au.

3.3. Feasibility of the sensor

We employed DPV as the tool to study the feasibility of the electrochemical nanoswitch biosensor in response to miRNA-21. RuHex, served as the signal reporter, can bind to the negatively charged DNA strands through electrostatic interaction. As can be seen in Fig. 2, the gold electrode modified by CP showed a very small DPV peak (curve a), because there were few RuHex cations binding to phosphate backbone through electrostatic interaction. In the absence of TP, LP or ORP + IRP could not directly hybridize with CP. Only another two similar small DPV peaks (curve b and c) were observed, which were attributed to nonspecific adsorption. However, when CP hybridized with TP, more RuHex positive ions were binding to CP and TP. A larger DPV peak current could be observed (curve d). The above phenomena showed that the sensor could be successfully constructed only in the presence of TP, while LP could be complementary with the exposed sticky end of CP. As a result of strands extended and binding of RuHex, the DPV peak (curve e) was slightly higher compared with curve d. When ORP + IRP (pH 6) was dropped on the gold surface which had been modified with LP/TP/CP, a significant DPV peak current (curve f) was observed. The remarkable signal amplification indicated that the continuous annular DNA nanoswitch had been successfully self-assembled by ORP + IRP

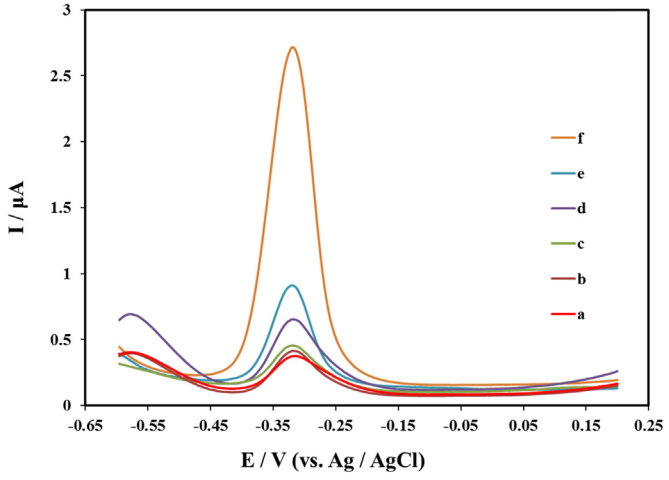

Fig. 2. Effect of various oligonucleotides modified on Au electrode on the DPV response currents: (a) CP, (b) LP/CP, (c) ORP + IRP/CP, (d) TP/CP, (e) LP/TP/CP, (f) ORP + IRP/LP/TP/CP. The concentration of miRNA-21 was 10 nM. The concentrations of IRP and ORP were 2 µM.

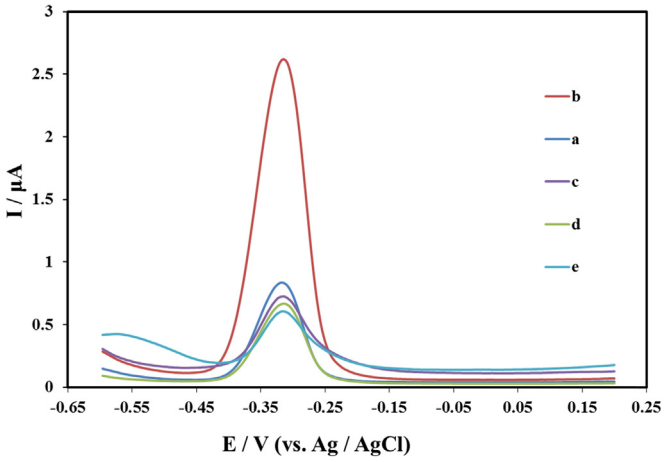

Fig. 3. DPV response of the biosensors self-assembled in H-buffers with different pH. (a) pH 5, (b) pH 6, (c) pH 7, (d) pH 8, (e) pH 9.

and bonded with a large number of RuHex. These outcomes indicated the viability of the proposed design for target detection.

3.4. DPV of different pH circumstance

The formation of this TFOs nanoswitch is pH-dependent, as a result of the Hoogsteen interaction. We explored the impact of various pH on the nanoswitch under the optimized experimental conditions. As shown in Fig. 3, when pH = 6, the DPV peak current was maximum (curve b), demonstrating that continuous annular DNA connected by TFOs is more likely to form under weak acid condition. More specifically, the protonation of cytosine residues can lead to the Hoogsteen base pairing between C-G•C+ triplets under weak acid conditions. Therefore, the IRP, ORP and another IRP can self-assemble to form a triple helix. Eventually, a good deal of electropositive RuHex will bind to the anionic phosphate through electrostatic adherence, producing a remarkably amplified electrochemical signal. On the contrary, while pH = 5, 7, 8 or 9, the peak current showed a distinct diminution (Corresponding curves a, c, d, e, respectively). The reason may be that the stabilization between C-G•C+ and T-A•T cannot reach equilibrium. Because C-G•C+ is stable under weak acid conditions and T-A•T prefers neutral conditions. Therefore, changing the acid-base environment can realize the switching of the nanoswitch and lead to different results.

3.5. Optimization of the experimental conditions

The main amplification and switch effect of this electrochemical biosensor comes from the continuous annular DNA. In order to fulfill the optimal experimental performance, experimental conditions such as amplification probes (ORP and IRP) concentration and hybridization time were studied respectively when the concentration of miRNA-21 was 10 nM. The impact of ORP and IRP concentrations (from 0 to 2.5 µM) on the electrochemical response is shown in Fig. S1A. The concentration of ORP was equal to the concentration of IRP. The hybridization time for self-assembly was 120 min. With the increase of the concentration of ORP and IRP, DPV peak current intensities were increased at first and then reached a platform at 2 µM, which was selected as the optimal concentration. As shown in Fig. S1B, the effect of hybridization time of ORP and IRP were also studied. The DPV signal increased gradually between 40 and 120 min and then reached a platform, indicating that the reaction reached equilibrium after 120 min. Therefore, the hybridization time was determined to be 120 min.

3.6. Analytical performance of the nanoswitch biosensor

To verify the analytical capability of the proposed method, the

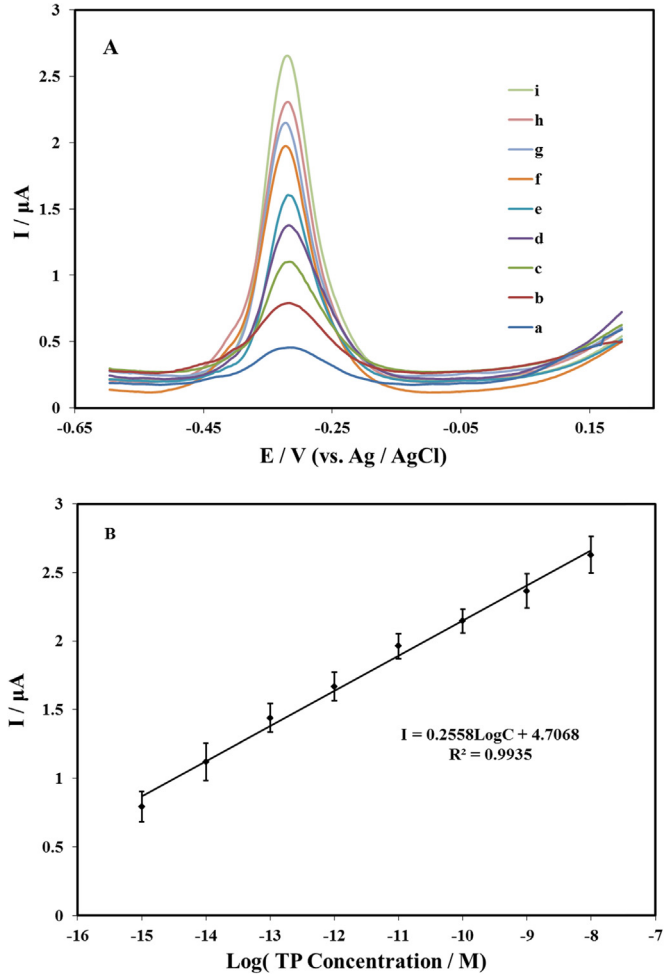

Fig. 4. (A) DPV response of the developed nanoswitch biosensor with different concentration of miRNA-21: (a) 0 M, (b) 1 fM, (c) 10 fM, (d) 100 fM, (e) 1 pM, (f) 10 pM, (g) 100 pM, (h) 1 nM, (i) 10 nM. (B) The linear relationship between the DPV peak current and the logarithm of miRNA-21 concentration ranging from 1 fM to 10 nM. The error bars indicate the standard deviations of three repetitive measurements.

nanoswitch biosensor was challenged by gradient concentrations of target miRNA-21 under optimal experimental conditions. According to Fig. 4A, DPV peak current gradually enhanced when the concentration of the target miRNA-21 increased from 0 M to 10 nM (curves a-i). The remarkable sensitivity can be attributed to the abundant of RuHex positive ions electrostatically bound to the continuous annular DNA. The electrical signal was amplified significantly. Fig. 4B shows the proportional relationship between target concentration and signal response. DPV peak currents showed a good linear dependence on the logarithm of miRNA-21 concentrations ranging from 1 fM to 10 nM. The linear equation for miRNA-21 detection is $y = 0.2558\text{LogC} + 4.7068$ (y is the DPV peak current and C is the concentration of target miRNA-21) with a correlation coefficient value (R^2) of 0.9935. The limit of detection (LOD), 0.84 fM, could be estimated by $3\sigma/S$ (σ is the standard deviation of the blank signal. S is the slope of the fit line). In addition, the reproducibility of the assay method was investigated. A relative standard deviation (RSD) of 5.1% corresponding to three repetitive measurements for 10 nM miRNA-21 was obtained, suggesting good reproducibility of the strategy.

3.7. Selectivity and stability of the proposed nanoswitch biosensor

Selectivity is an essential element for a good biosensor. Consequently, different miRNAs, including miRNA-141, miRNA-199a, single-base mismatched, and two-base mismatched miRNA-21 sequences, were employed as the interfering material to study the selectivity of the biosensor. As illustrated in Fig. S2, the DPV peak current intensity of the proposed method was increased significantly in the presence of miRNA-21 (10 nM) compared to the blank solution (no target miRNA-21). However, when the miRNA-141 (1 μM), miRNA-199a (1 μM), single-base mismatched miRNA-21 (1 μM), and two-base mismatched miRNA-21 (1 μM) were used to substitute the target miRNA-21 respectively, there was no significant increase in the DPV signal of these interfering substances compared to the blank. After blending the miRNA-141 (1 μM), miRNA-199a (1 μM), single-base mismatched miRNA-21 (1 μM) and two-base mismatched miRNA-21 (1 μM) with the target miRNA-21 (10 nM), the DPV showed a tremendous current intensity and no obvious difference from that of only 10 nM miRNA-21 could be observed. The results showed that the proposed method exhibited excellent selectivity. The stability of the proposed nanoswitch biosensor was also verified by storing at 4 °C and measuring every 12 h. The results (Fig. S3) showed that after 72 h, the DPV response of the biosensor retained about 84.7% of its original response, indicating the satisfactory stability of the proposed biosensor.

3.8. Application of the nanoswitch biosensor in human serum

In order to study the applicability of the proposed DNA nanoswitch in actual samples, we conducted the following experiments. We tested miRNA-21 levels in serum samples from 6 breast cancer patients and 6 healthy volunteers, respectively. As presented in Table 1, the DPV peak currents of patients' serum were obviously higher than those of the healthy donors', which was consistent with reported literatures (Oudeng et al., 2018; Shi et al., 2015). As references, a commercial qRT-PCR kit was simultaneously used to quantify the serum miRNA-21expression levels. The results acquired by our proposed method are very consistent with the results obtained with qRT-PCR on the same samples (Fig. S4). Hence, the results showed that the proposed strategy can ultra-sensitively detect targets in complicated biological samples and have considerable potential in clinical diagnosis and prognostic evaluation.

4. Conclusions

In summary, we developed a novel self-assembled pH-sensitive continuous circular DNA nanoswitch biosensor for ultrasensitive electrochemical detection of miRNA-21. The DNA nanoswitch biosensor is simple and inexpensive, without the need for enzyme, label, or complex operation. What's more, only in a weakly acidic environment (pH = 6) will the nanoswitch biosensor be activated, allowing a significant signal to be detected. The biosensor shows high selectivity and is able to quantify miRNA-21 down to 0.84 fM. Besides, this approach can directly evaluate miRNA-21 in complex biological samples without pretreatment, which reduces the complexity of the experiment greatly and makes it possible for this nanoswitch biosensor to be used for clinical diagnosis and prognostic evaluation in future.

CRediT authorship contribution statement

Xian Chen: Conceptualization, Methodology, Writing - review & editing. **Le Yao:** Investigation, Methodology, Writing - review & editing. **Yu-Chao Wang:** Investigation. **Qin Chen:** Investigation. **Hai Deng:** Writing - review & editing. **Zhen-Yu Lin:** Writing - review & editing. **Huang-Hao Yang:** Supervision.

Acknowledgment

This work was financially supported by China Scholarship Council, China (grant no. 201706655025), Department of Education, Fujian

Table 1
MiRNA-21 assay in human serum (n = 3) with the proposed nanoswitch biosensor.

Breast cancer patients	DPV response (μA)	Average value(μA)	RSD	Healthy donors	DPV response (μA)	Average value(μA)	RSD
1	1.72	1.60	0.057	1′	1.34	1.19	0.097
	1.58				1.06		
	1.50				1.17		
2	1.45	1.53	0.040	2′	1.29	1.12	0.108
	1.60				1.02		
	1.54				1.05		
3	1.59	1.54	0.041	3′	1.09	1.13	0.125
	1.45				0.98		
	1.58				1.32		
4	1.47	1.59	0.067	4′	0.85	1.02	0.126
	1.57				1.16		
	1.73				1.05		
5	1.36	1.43	0.106	5′	1.26	1.07	0.128
	1.64				0.94		
	1.29				1.01		
6	1.54	1.37	0.108	6′	1.02	1.17	0.136
	1.18				1.39		
	1.39				1.10		

Province, China (grant no. JK2017006) and National Natural Science Foundation of China, China (grant no. 21575027).

Declaration of interests

None.

Appendix A. Supporting information

Supplementary data associated with this article can be found in the online version at doi:10.1016/j.bios.2019.02.004.

References

Bartel, D.P., 2014. Cell 116, 281–297.
Chen, X., Hong, C.Y., Lin, Y.H., Chen, J.H., Chen, G.N., Yang, H.H., 2012. Anal. Chem. 84, 8277–8283.
Chen, X., Lin, Y.H., Li, J., Lin, L.S., Chen, G.N., Yang, H.H., 2011. Chem. Commun. 47, 12116–12118.
Desrosiers, A., Vallée-Bélisle, A., 2017. Nanomedicine 12, 175–179.
Fang, C.S., Kim, K.S., Ha, D.T., Kim, M.S., Yang, H., 2018. Anal. Chem. 90, 4776–4782.
Hansen, T.F., Kjær-Frifeldt, S., Christensen, R.D., Morgenthaler, S., Blondal, T., Lindebjerg, J., Sørensen, F.B., Jakobsen, A., 2014. Br. J. Cancer 111, 1285–1292.
Hessam, S., Sand, M., Skrygan, M., Gambichler, T., Bechara, F.G., 2017. Inflammation 40, 464–472.
Hu, L., Stasheuski, A.S., Wegman, D.W., Wu, N., Yang, B.B., Hayder, H., Peng, C., Liu, S.K., Yousef, G.M., Krylov, S.N., 2017. Anal. Chem. 89, 4743–4748.
Huang, F.J., Liao, W.C., Sohn, Y.S., Nechushtai, R., Lu, C.H., Willner, I., 2016. J. Am. Chem. Soc. 138, 8936–8945.
Iacovelli, F., Idili, A., Benincasa, A., Mariottini, D., Ottaviani, A., Falconi, M., Ricci, F., Desideri, A., 2017. J. Am. Chem. Soc. 139, 5321–5329.
Idili, A., Vallee-Belisle, A., Ricci, F., 2014. J. Am. Chem. Soc. 136, 5836–5839.
Jin, S., Murtaw, M.D., Chen, H.X., Lamb, D.T., Ferguson, S.A., Arvin, N.E., Dawod, M., Kennedy, R.T., 2016. Anal. Chem. 88, 6703–6710.
Jung, S., Kim, J., Lee, D.J., Oh, E.H., Lim, H., Kim, K.P., Choi, N., Kim, T.S., Kim, S.K., 2016. Sci. Rep. 6, 22975.
Kulcheski, F.R., Marcelino-Guimaraes, F.C., Nepomuceno, A.L., Abdelnoor, R.V., Margis, R., 2010. Anal. Biochem. 406, 185–192.
Le, B.H., Seo, Y.J., 2018. Bioorg. Med. Chem. Lett. 28, 2035–2038.
Lee, J.M., Jung, Y., 2011. Angew. Chem. Int. Ed. 50, 12487–12490.
Li, Z.H., Zhao, B., Wang, D.F., Wen, Y.L., Liu, G., Dong, H.Q., Song, S.P., Fan, C.H., 2014. ACS Appl. Mater. Interfaces 6, 17944–17953.
Liao, W.C., Willner, I., 2017. Adv. Funct. Mater. 27, 1702732.
Lim, D., Byun, W.G., Koo, J.Y., Park, H., Park, S.B., 2016. J. Am. Chem. Soc. 138, 13630–13638.
Lin, M.H., Wang, J.J., Zhou, G.B., Wang, J.B., Wu, N., Lu, J.X., Gao, J.M., Chen, X.Q., Shi, J.Y., Zuo, X.L., Fan, C.H., 2015. Angew. Chem. Int. Ed. 54, 2151–2155.
Liu, B.Q., Zhang, B., Chen, G.N., Yang, H.H., Tang, D.P., 2014. Biosens. Bioelectron. 53, 390–398.
Liu, H.Y., Tian, T., Zhang, Y.H., Ding, L.H., Yu, J.H., Yan, M., 2017. Biosens. Bioelectron. 89, 710–714.
Lu, T.X., Rothenberg, M.E., 2017. J. Allergy Clin. Immunol. 2017 (141), 1202–1207.
Modi, S., Nizak, C., Surana, S., Halder, S., Krishnan, Y., 2013. Nat. Nanotechnol. 8, 459–467.
Modi, S., Swetha, M.G., Goswami, D., Gupta, G.D., Mayor, S., Krishnana, Y., 2009. Nat. Nanotechnol. 4, 325–330.
Oudeng, G., Au, M., Shi, J.Y., Wen, C.Y., Yang, M., 2018. ACS Appl. Mater. Interfaces 10, 350–360.
Qian, R.C., Cao, Y., Long, Y.T., 2016. Anal. Chem. 88, 8640–8647.
Raftery, R.M., Walsh, D.P., Castaño, I.M., Heise, A., Duffy, G.P., Cryan, S.A., O'Brien, F.J., 2016. Adv. Mater. 28, 5447–5469.
Sheu, S.Y., Grabellus, F., Schwertheim, S., Worm, K., Broecker-Preuss, M., Schmid, K.W., 2010. Br. J. Cancer 102, 376–382.
Shi, K., Dou, B.T., Yang, C.Y., Chai, Y.Q., Yuan, R., Xiang, Y., 2015. Anal. Chem. 87, 8578–8583.
Smith, D., Schuller, V., Engst, C., Rädler, J., Lidel, T., 2013. Nanomedicine 8, 105–121.
Tian, T., Wang, J.Q., Zhou, X., 2015. Org. Biomol. Chem. 13, 2226–2238.
Válóczi, A., Hornyik, C., Varga, N., Burgyán, J., Kauppinen, S., Havelda, Z., 2004. Nucleic Acids Res. 32, e175–e181.
Várallyay, É., Burgyán, J., Havelda, Z., 2008. Nat. Protoc. 3, 190–196.
Wang, L., Su, D.D., Berry, S.N., Lee, J., Chang, Y.T., 2017. Chem. Commun. 53, 12465–12468.
Wang, Z.X., Bian, H.B., Wang, J.R., Cheng, Z.X., Wang, K.M., 2011. J. Surg. Oncol. 104, 847–851.
Wei, T.X., Du, D., Wang, Z.Y., Zhang, W.W., Lin, Y.H., Dai, Z.H., 2017. Biosens. Bioelectron. 94, 56–62.
Xiong, E.H., Li, Z.Z., Zhang, X.H., Zhou, J.W., Yan, X.X., Liu, Y.Q., Chen, J.H., 2017. Anal. Chem. 89, 8830–8835.
Xu, J.H., Zhao, J.M., Evan, G.H., Xiao, C.Y., Cheng, Y., Xiao, J.J., 2012. J. Mol. Med. 90, 865–875.
Xu, M.D., Zhuang, J.Y., Chen, X., Chen, G.N., Tang, D.P., 2013. Chem. Commun. 49, 7304–7306.
Xu, X.W., Wang, L., Li, K., Huang, Q.H., Jiang, W., 2018. Anal. Chem. 90, 3521–3530.
Xu, Z.Q., Liao, L.L., Chai, Y.Q., Wang, H.J., Yuan, R., 2017. Anal. Chem. 89, 8282–8287.
Yin, B.C., Liu, Y.Q., Ye, B.C., 2012. J. Am. Chem. Soc. 134, 5064–5067.
Yu, S., Wang, Y.Y., Jiang, L.P., Bi, S., Zhu, J.J., 2018. Anal. Chem. 90, 4544–4551.
Zaman, M.S., Chauhan, N., Yallapu, M.M., Gara, R.K., Maher, D.M., Kumari, S., Sikander, M., Khan, S., Zafar, N., Jaggi, M., Chauhan, S.C., 2016. Sci. Rep. 6, 20051.
Zhang, J., Wang, L.L., Hou, M.F., Xia, Y.K., He, W.H., Yan, A., Weng, Y.P., Zeng, L.P., Chen, J.H., 2018. Biosens. Bioelectron. 102, 33–40.
Zhao, Y., Cao, L., Ouyang, J., Wang, M., Wang, K., Xia, X.H., 2013. Anal. Chem. 85, 1053–1057.
Zhou, B.C., Yang, H.W., Deng, Y., Liu, M., Liu, B., He, N.Y., Li, Z.Y., 2016. Sci. China Chem. 59, 1051–1058.